ACS APPLIED MATERIALS & INTERFACES

Research Article

www.acsami.org

# Controlled Synthesis of Carbon-Coated Cobalt Sulfide Nanostructures in Oil Phase with Enhanced Li Storage Performances

Wenhui Shi,[†] Jixin Zhu,[†] Xianhong Rui,[†] Xiehong Cao,[†] Charlotte Chen,[†] Hua Zhang,[†] Huey Hoon Hng,[†] and Qingyu Yan*[,†,‡,§]

[†]School of Materials Science and Engineering, Nanyang Technological University, Singapore 639798, Singapore

[‡]Energy Research Institute, Nanyang Technological University, 637459, Singapore

[§]TUM CREATE Centre for Electromobility, Singapore 637459, Singapore

Supporting Information

**ABSTRACT:** A novel solvothermal process was developed for the synthesis of carbon-coated $Co_9S_8$ nanodandelions using 1-dodecanethiol as the sulfur source and the soft template. Replacing 1-dodecanethiol with sulfur powder as the sulfur source leads to the formation of 20 nm $Co_9S_8$ nanoparticles without carbon coating. When tested as LIB anode, the C@$Co_9S_8$ dandelion delivers a specific capacity of 520 mA h $g^{-1}$ at a current density of 1 A $g^{-1}$ (1.8 *C*) during the 50th cycle, which is much higher than that of $Co_9S_8$ nanoparticles (e.g. 338 mA h $g^{-1}$). Furthermore, the C@$Co_9S_8$ dandelion also exhibits excellent high *C*-rate performance, e.g., depicts a 10th-cycle capacity of 373 mA h $g^{-1}$ at a current density of 6 A $g^{-1}$ (10.9 *C*), which is better than that of many reported anode materials. Such synthesis approach is attractive for the preparation of sulfide anode materials with high Li storage properties.

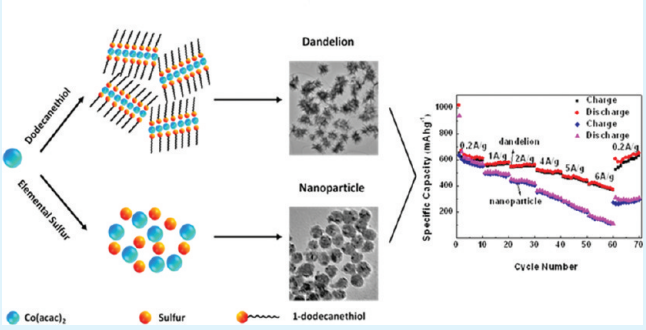


**KEYWORDS:** *cobalt sulfides, solvothermal, carbon coating, dandelion, nanoparticles, LIB*

## INTRODUCTION

Lithium-ion batteries (LIBs) have been widely used in portable electronic devices and regarded as the most promising candidate for the power sources of electric vehicles (EVs).[1−8] Recently, much effort has been devoted to seeking new materials as anodes for next-generation LIBs,[9−11] which can deliver higher capacities than graphite while exhibiting excellent cyclability. Transition metal sulfides as alternative anode materials have attracted considerable interest because of their high theoretical capacities.[12,13] On the basis of the Li storage mechanism, these metal sulfides can be generally categorized into two types: (1) insertion-reaction based and (2) conversion-reaction based. For the former type, energy is stored by Li insertion−desertion process, such as $MoS_2$,[14−16] $WS_2$,[17] $ZrS_2$[18] etc. This type of sulfides normally has low theoretical capacities from reversible Li insertion−desertion reaction. For example, the maximum theoretical capacity of $MoS_2$ is 167 mA h $g^{-1}$ based on the reaction of $MoS_2$ + Li ↔ Li*x*$MoS_2$ ($0 \le x \le 1$), but these materials are also reported to exhibit higher specific capacities because of the involvement of conversion reactions.[14−16] The conversion-reaction based metal sulfides (M−S, where M = Fe, Co, Ni, etc.) go through redox-reaction to store Li and show higher theoretical capacities.[19−22] One major issue relates to the sulfides anodes is the pulverization of electrodes due to the large volume changes upon discharge/charge, which causes fast decay of the specific capacities. Construction of nanoscaled materials is an effective approach to buffer the volume strain and improve the cyclability.[23−26] It also leads to the advantages of (1) increasing the interaction area between the active material and the electrolyte, and (2) shortening the diffusion paths of $Li^+$, which may result in improved rate capabilities.[27,28]

Besides the pulverization of electrodes, another main concern for conversion-reaction based sulfide anodes is the formation of polysulfide anions, which is soluble in the polar organic solvents used in electrolytes.[29−31] The dissolution of polysulfide would lead to decrease in the conductivity of electrolyte.[32] Moreover, during cycling the dissolved polysulfide anions can migrate through the separator to reach the cathode side, which leads to poor cyclability of the LIBs.[33] A recent report[34] on Li−S battery demonstrated that cathodes based on nanostructured sulfur embedded in mesoporous carbon exhibited high reversible capacity and good rates, which is mainly due to the porous carbon that could absorb and trap the polysulfides. Such a strategy should be promising if extended to improve the Li storage properties of conversion-reaction-based sulfide anodes in LIBs.[22,23,35]

**Received:** February 29, 2012
**Accepted:** May 16, 2012
**Published:** May 21, 2012

   dx.doi.org/10.1021/am3003654 | *ACS Appl. Mater. Interfaces* 2012, 4, 2999−3006

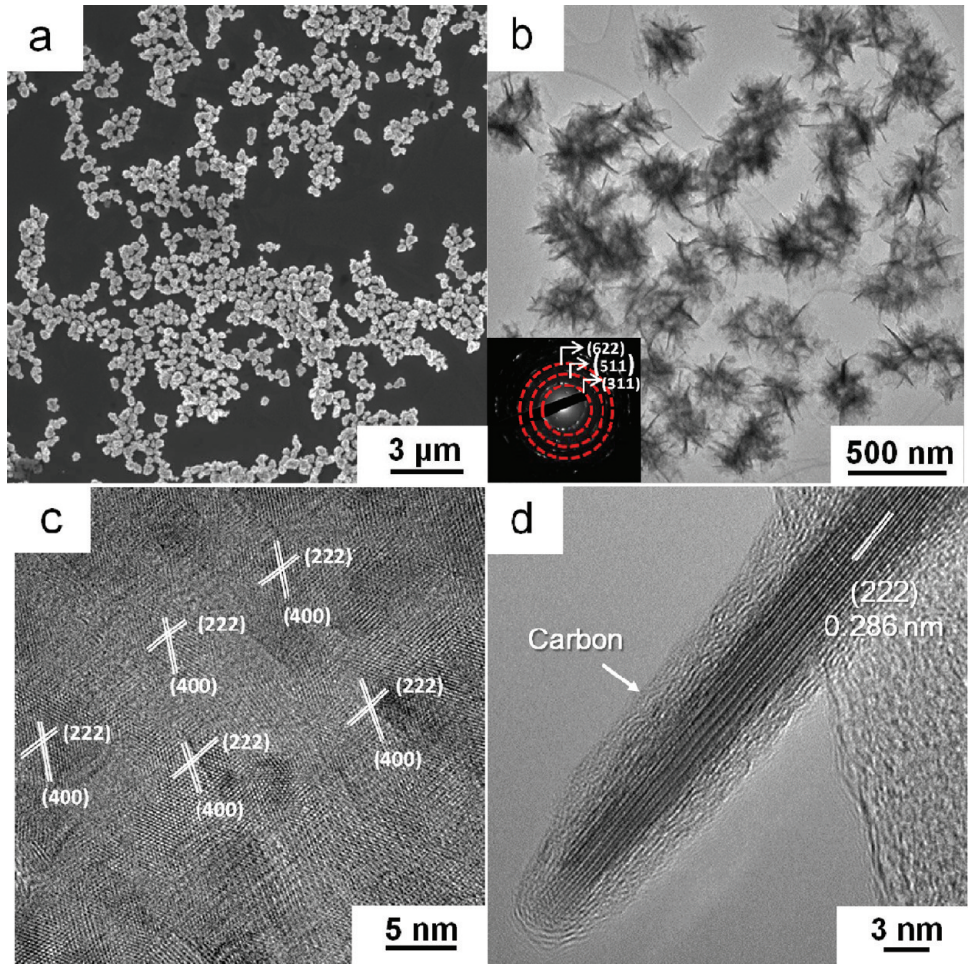


**Figure 1.** (a) Low-magnification SEM image, (b) low-magnification TEM image of the $Co_9S_8$ dandelions, (c) top-view and (d) side-view HRTEM imgaes of a nanosheet in the $Co_9S_8$ dandelion. The SAED pattern is shown in inset of b.

Along with many other metal sulfides, cobalt sulfides are considered as promising electrodes for lithium batteries for their low cost and high theoretical capacity. Up to now, different cobalt sulfide nanostructures have been reported.[20,36−40] However, the controlled synthesis of cobalt sulfides with satisfied Li storage properties still faces great challenges. Herein, we show a novel solvothermal process in oleylamine to grow carbon coated cobalt sulfide ($Co_9S_8$) nanosheets ($C@Co_9S_8$) using 1-dodecanethiol as (1) the sulfur source, (2) the carbon source and (3) the soft template. With the assistance of oleic acid, the $C@Co_9S_8$ form dandelion-shaped nanostructures. When elemental sulfur was used to replace 1-dodecanethiol as sulfur source, it resulted in the growth of 20 nm $Co_9S_8$ nanoparticles ($Co_9S_8$ NPs) without the carbon layer. When tested as LIB anode, the $C@Co_9S_8$ dandelion delivered a specific capacity of 520 mA h $g^{-1}$ at a current density of 1 A $g^{-1}$ (1.8 *C*) during the 50th cycle, which is much higher than that of $Co_9S_8$ NPs (e.g. 338 mA h $g^{-1}$ at 1.8 *C* during the 50th cycle) and comparable with the theoretical capacity of $Co_9S_8$ (539 mA h $g^{-1}$). Furthermore, the $C@Co_9S_8$ dandelion also exhibited excellent rate performance, e.g., depicts a 10th-cycle capacity of 373 mA h $g^{-1}$ at a current density of 6 A $g^{-1}$ (10.9 C). Such synthesis approach is attractive for developing sulfide anode materials with high Li storage properties.

## EXPERIMENTAL SECTION

**Synthesis of $Co_9S_8$ Dandelion.** In a typical synthesis, 0.2 mmol cobalt(II) acetylacetonate $Co(acac)_2$, 1 ml oleic acid (3 mmol), and 5 ml oleylamie were added into a 50 mL three-necked flask. The solution was stirred at 100 °C under Ar flow for 30 mins. After dissolving, 1 mL of 1-dodecanethiol was added into the flask and then the temperature of the mixture was increased to 230 °C. The solution was refluxed at 230 °C for 10 mins and then cooled down to room temperature. The dark precipitates were cleaned by repeated washing with hexane and centrifuging several times. After being dried in a vacuum oven at 50°C for 4 h, the samples were annealed under an Ar atmosphere at 350 °C for 1 h to improve the crystallinity.

**Synthesis of $Co_9S_8$ Nanoparticles.** 0.5 mmol of cobalt(II) acetylacetonate $Co(acac)_2$ was dispersed in 5 mL of oleylamine in a 50 mL three-necked flask equipped with a condenser and thermometer. The solution was stirred at 100 °C under Ar flow for 30 min. After that, the solution was heated to 200 °C and a solution of 0.5 mmol of sulfur dissolved in 5 mL of oleylamine was then quickly injected into the flask. The solution turned dark immediately after injection and the nanocrystals were allowed to grow at 200 °C for 10 mins and then cooled to room temperature. The precipitates were collected and purified by washing with hexane and centrifuging. After drying in vacuum oven at 50 °C for 4 h, the samples were annealed under Ar atmosphere at 350 °C for 1 h to improve the crystallinity.

**Characterization.** The morphology of the samples was investigated using a field-emission scanning electron microscope (JEOL, Model JSM-7600F). Transmission electron microscope (TEM) images were taken on a JEOL 2010F (equipped with EDX) operating at 200 kV. The crystal structural characterization of the samples was carried

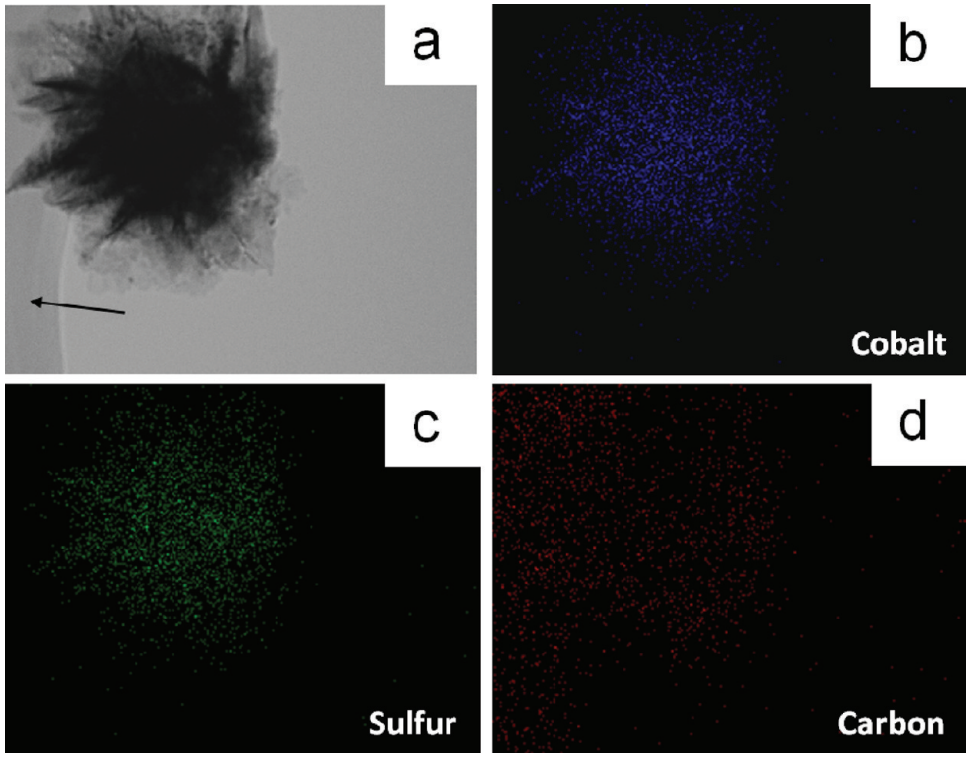


**Figure 2.** Elemental mapping of $Co_9S_8$ dandelion: (a) bright-field TEM image, (b) cobalt map, (c) sulfur map, and (d) carbon map. Black arrow indicates carbon fiber support of TEM grid.

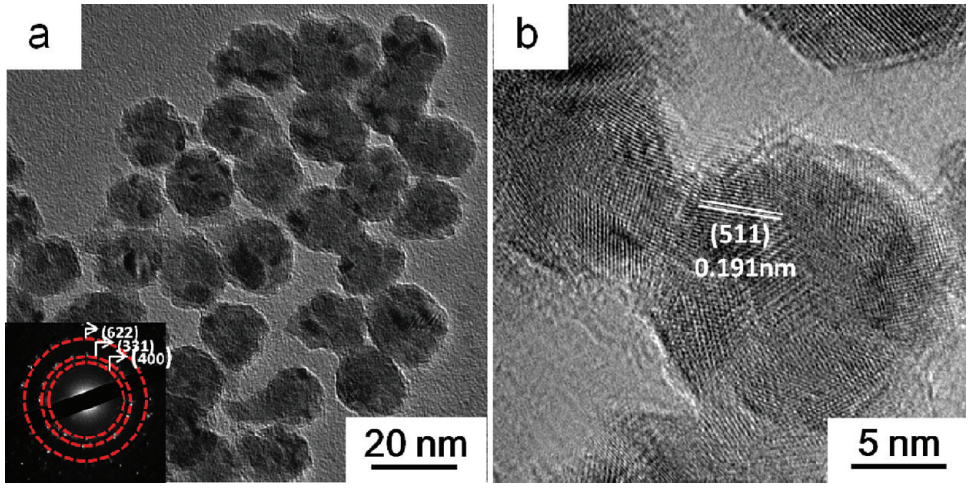


**Figure 3.** (a) TEM and (b) HRTEM images of $Co_9S_8$ nanopartcles. The inset in a is the corresponding SAED pattern.

out on a Shimadzu 6000 X-ray diffractometer at a scan rate of 1°/min with the $2\theta$ range from 10 to 80° by using Cu $K\alpha_1$ ($\lambda$ = 0.15406 nm) radiation. The Raman spectra were obtained by using WITec CRM200 confocal Raman microscopy system with a laser wavelength of 488 nm and spot size of 0.5 nm. To calibrate the wavenumber, the Si peak at 520 $cm^{-1}$ was used as a reference. The specific surface areas were investigated by using the Brunauer–Emmet–Teller (BET) methods.

**Evaluation of Electrochemical Properties.** The working electrode was fabricated by combining the cobalt sulfide samples with conductive carbon blacks and polyvinylidene fluoride (PVDF) binder in a weight ratio of 8:1:1. The slurry was coated on a copper foil and dried overnight in a vacuum oven at 60 °C. The electrochemical measurements were carried out using two-electrode coin cells (X2 Labwares, Singapore) with pure lithium foil as both the counter and the reference electrodes at room temperature. The electrolyte used was 1 M LiPF6 in ethylene carbonate (EC)/diethyl carbonate (DEC) (1:1 in volume). Cell assembly was carried out in an Ar-filled glovebox with concentrations of moisture and oxygen below 1.0 ppm. The galvanostatic discharge/charge tests were performed using a NEWARE battery tester at different current rates with a voltage window of 0.01–3 V. Cyclic voltammogram (CV) and electrochemical impedance spectrum (EIS) were performed on CHI 660C electrochemical station.

## ■ RESULTS AND DISCUSSION

The crystal structures of the cobalt sulfide samples prepared with 1-dodecanethiol or sulfur powder after annealing at 350°C under Ar atmosphere were examined using x-ray diffraction (XRD). The XRD patterns (see the Supporting Information, Figure S1) reveal the formation of face-centered cubic (fcc) $Co_9S_8$ (JCPDS card no. 65-1765) in both samples with no detectable impurity phase.


dx.doi.org/10.1021/am3003654 | ACS Appl. Mater. Interfaces 2012, 4, 2999–3006

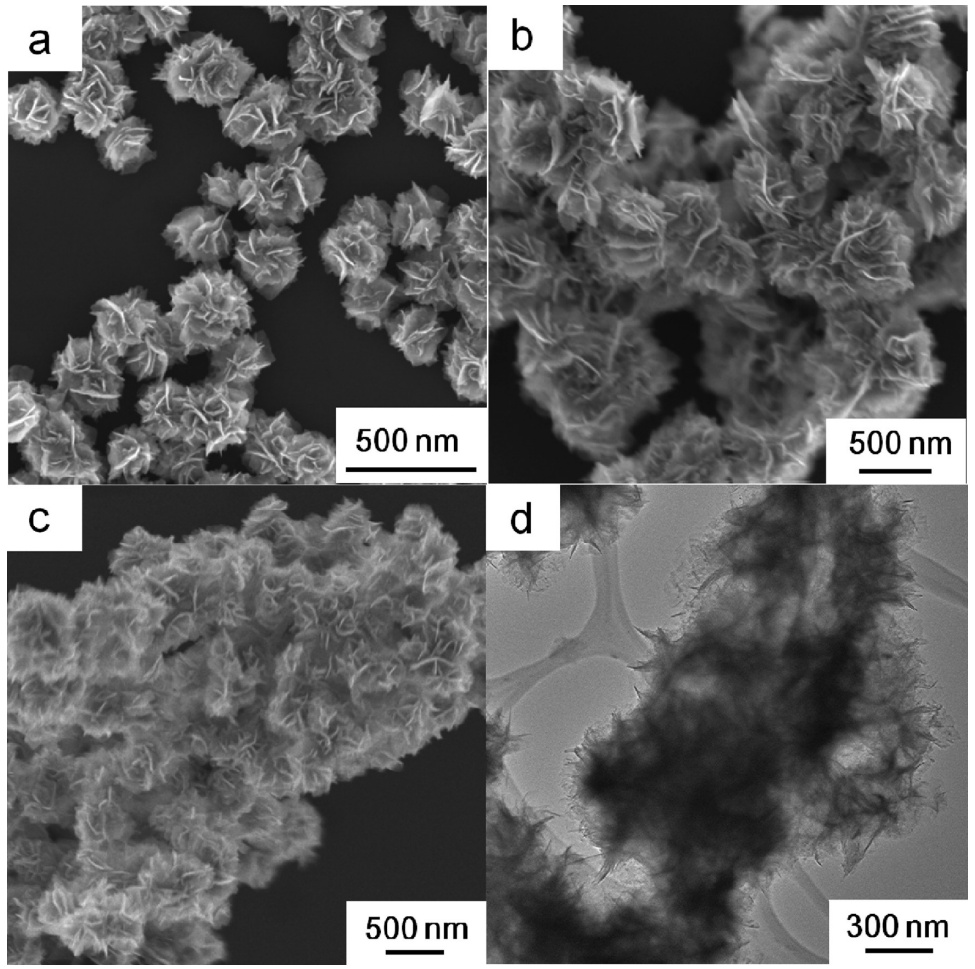


**Figure 4.** SEM images of $Co_9S_8$ nanostructures prepared with (a) $I_{oleic/Co}$ = 15, (b) $I_{oleic/Co}$ = 8, (c) $I_{oleic/Co}$ = 0. (d) TEM image of $Co_9S_8$ nanostructures with $I_{oleic/Co}$ = 0.

The SEM and TEM images (Figure 1a,b) display the typical morphology of the sample prepared using 1-dodecanethiol as the sulfur source with a molar ratios $I_{oleic/Co}$ = oleic acid:$Co(acac)_2$ = 15, which is dandelion-shaped nanostructures with an average size of ~250 nm. The nanodandelions show no obvious coarsening although they have been annealed at 350°C under Ar atmosphere for 1 h. The corresponding selected-area electron diffraction (SAED) measurement (inset in Figure 1b) of a single dandelion shows the ring pattern, which confirms the formation of fcc $Co_9S_8$. Such observation is consistent with the XRD result. The high resolution TEM images (Figure 1c,d) indicate that the individual $Co_9S_8$ dandelion is composed of thin nanosheets with the thickness of <5 nm. The nanosheet in the $Co_9S_8$ dandelion is polycrystalline and composed of nanograins of 4−8 nm (Figure 1c) with the preferred exposure of (0, 1, −1) facets. The side-view HRTEM image (Figure 1d) indicates that there is a thin amorphous layer coated on the nanosheet in the $Co_9S_8$ dandelion. The selected area elemental mapping (Figure 2) of one $Co_9S_8$ dandelion reveals that other than the presence of Co and S element, there are considerable amount of carbon uniformly distributed in the sample. The Raman spectrum of the $Co_9S_8$ dandelions (see the Supporting Information, Figure S2) shows two broad resonance peaks located at ~1350 $cm^{-1}$ (D band) and ~1580 $cm^{-1}$ (G band), which is similar to those previously reported[41] for amorphous carbon materials. Thus, the amorphous layer on the nanosheets in the $Co_9S_8$ dandelion is believed to be amorphous carbon, which leads to the conclusion that the sample is carbon coated $Co_9S_8$ dandelion (named as C@$Co_9S_8$ dandelion). The carbon coating is assumed to be due to the carbonization of organic molecules in the annealing process.

To understand the formation of the C@$Co_9S_8$ dandelions, we used sulfur powder as the sulfur source instead of 1-dodecanethiol. The synthesis was carried out without the addition of oleic acid. The XRD pattern of the sample reveals that it is fcc $Co_9S_8$ (JCPDS card no. 65-1765) with no detectable impurity phase. The TEM image (Figure 3a) shows that the sample is quasi-spherical nanoparticles with an average size of ~20 nm. The annealing process at 350°C under Ar atmosphere did not cause any obvious coarsening of the particles although partial agglomeration between particles was observed. The SAED pattern of the nanoparticles confirms the formation of fcc $Co_9S_8$, which is consistent with the XRD result. The HRTEM image (Figure 3b) reveals that these $Co_9S_8$ nanoparticles are polycrystalline with grain sizes of 5-8 nm. Interestingly, there is no noticeable amorphous carbon layer on these $Co_9S_8$ nanoparticles and the Raman spectrum of the nanoparticles shows no detectable D or G band (see the Supporting Information, Figure S2). These observations support the assumption that the amorphous carbon layer is due to the carbonization of surface organic molecules, e.g., 1-dodecanethiol and/or oleic acid, during the annealing process.

**Scheme 1. Illustration of the Typical Preparation Routes and the Proposed Formation Mechanisms of C@$Co_9S_8$ Dandelion and $Co_9S_8$ Nanoparticles**

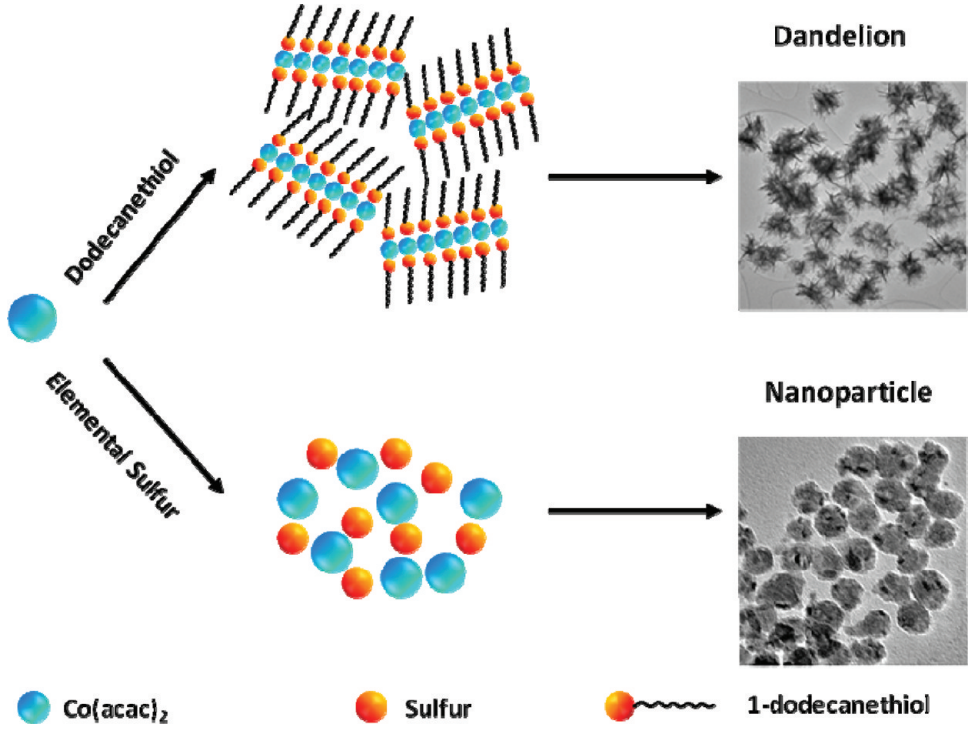


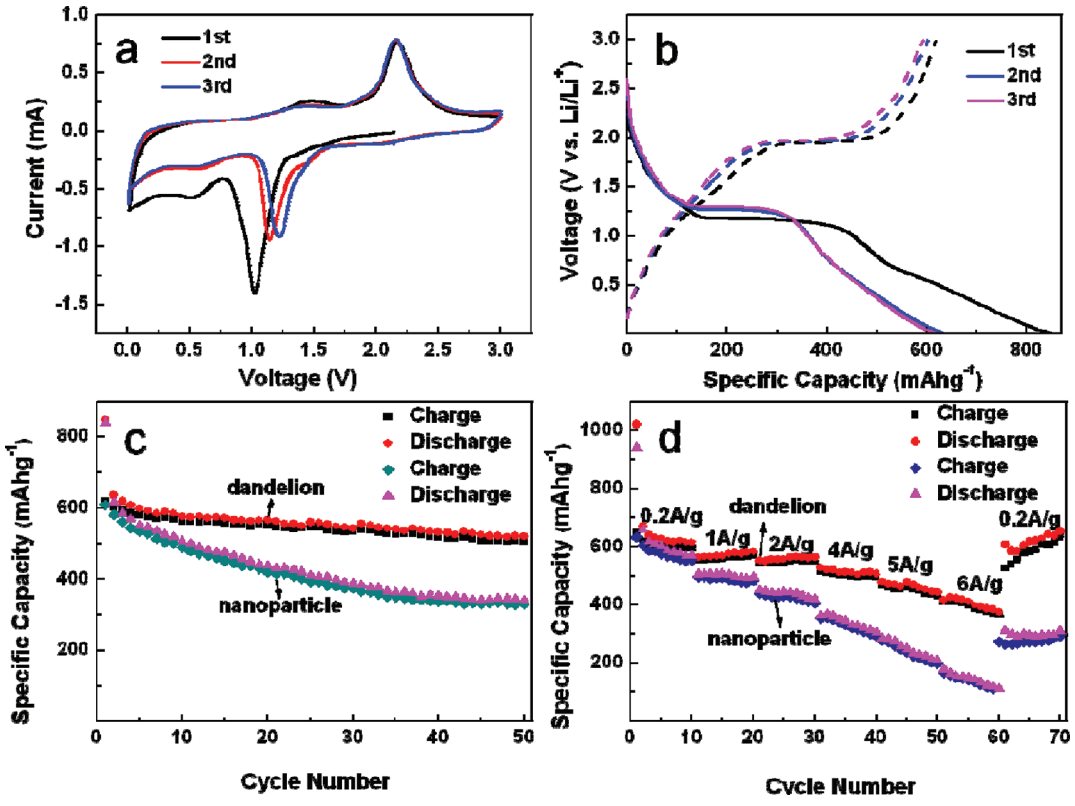


**Figure 5.** (a) Representative cyclic voltammograms of C@$Co_9S_8$ dandelion for the 1st, 2nd, and 3rd cycles at a scan rate of 0.5 mV $s^{-1}$ between 0.01 V and 3 V. (b) Discharge/charge voltage profiles of C@$Co_9S_8$ dandelion for the 1st, 2nd, and 3rd cycles. (c) Comparative cycling performance of C@$Co_9S_8$ dandelion and $Co_9S_8$ nanoparticles at a current density of 1 A $g^{-1}$. (d) Cycling stabilities of C@$Co_9S_8$ dandelion and $Co_9S_8$ nanoparticles at various current densities.

To verify the role of oleic acid, we also carried out preparation of $Co_9S_8$ using 1-dodecanethiol as the sulfur sources with different values of $I_{oleic/Co}$. The SEM images (Figure 4a–c) reveal that the morphology of $Co_9S_8$ depends on


dx.doi.org/10.1021/am3003654 | ACS Appl. Mater. Interfaces 2012, 4, 2999–3006

the values of $I_{oleic/Co}$. With decreasing value of $I_{oleic/Co}$, the samples changed from nanodandelions ($I_{oleic/Co}$ = 15) to agglomerated clusters of nanosheets ($I_{oleic/Co}$ = 0). TEM image of sample of $I_{oleic/Co}$ = 0 (Figure 4d) demonstrates that the thickness of a single nanosheet shows no noticeable change as compared to that of sample prepared with $I_{oleic/Co}$ = 15. Thus, the oleic acid is suggested to be important in confining the aggregation of nanosheets and leading to the formation of nanodandelions.

To further study the formation process of C@$Co_9S_8$, we also conducted a time-dependent experiment (see the Supporting Information, Figure S4). On the basis of the above observation, the proposed formation process of C@$Co_9S_8$ nanodandelions is illustrated in Scheme 1. For layer-structured sulfides, e.g., $MoS_2$,[14−16] $WS_2$,[17] $ZrS_2$,[18]CoS,[42] growth of 2D nanosheets or nanoplates have been reported, which is mainly due to confined growth within (001) planes of such hexagonal symmetric crystal structure. The cubic symmetric crystal structure of $Co_9S_8$, however, may not facilitate the growth of such 2D nanostructures. Although it has been demonstrated that oriented attachment of cubic-symmetry PbS nanocrystals can lead to the formation of single crystalline nanosheets,[43] the polycrystalline nature of the nanosheets in the $Co_9S_8$ dandelion indicates that the growth of such 2D nanostructures may be mainly due to the template effect of surfactants instead of the crystal structure. It is suggested that the formation of nanosheets in the $Co_9S_8$ dandelion is due to the lamellar assemblies of 1-dodecanethiol as illustrated in Scheme 1. The thiol head group in 1-dodecanethiol molecular can strongly bond to Co in $Co(acac)_2$, which forms $Co_9S_8$ under high temperature. The alkyl chains of the 1-dodecanethiol may be converted to amorphous carbon during the annealing process and remained on the surface of the nanosheets in the $Co_9S_8$ dandelion. The oleic acid with proper concentration in the solution can form secondary micelles to induce the growth of the dandelion shape by folding these $Co_9S_8$ nanosheets together. For the synthesis process using sulfur powder as the sulfur source and without the addition of oleic acid, the growth of $Co_9S_8$ nanoparticles is mainly due to the lack of lamellar templates formed by 1-dodecanethiol molecules. Also, the olylamine molecules may only weakly interact with $Co_9S_8$, which can be easily removed during the washing and annealing process. Thus, the surface of the $Co_9S_8$ nanoparticles is relatively clean without noticeable carbon layers.

The $N_2$ gas adsorption−-desorption isotherms were also measured for the C@$Co_9S_8$ dandelion and $Co_9S_8$ nanoparticles (see the Supporting Information, Figure S3). The specific surface area of C@$Co_9S_8$ dandelion is estimated to be ∼76 $m^2$/g based on the Brunauer−Emmett−Teller (BET) analysis (see the Supporting Information, Figure S3), which is 62% higher than that of $Co_9S_8$ nanoparticles (e.g., 47 $m^2$/g).

The electrochemical properties of C@$Co_9S_8$ dandelion and $Co_9S_8$ nanoparticles were investigated as anode materials of LIB based on the half cell configuration.[44,45] Figure 5a shows the representative cyclic voltammetry (CV) curves of C@$Co_9S_8$ dandelion for the 1st, 2nd, and 3rd discharge−charge cycles, respectively. A strong reduction peak in the cathodic sweep at ∼1 V corresponds to the reaction:[46,47] $Co_9S_8$ + 16 Li ↔ 8 $Li_2S$ + 9 Co. Such peak also exists in the next two discharge curves although slightly shifted to the higher potential range. The weak and broad peak at ∼0.5 V is ascribed to the decomposition of the electrolyte and the formation of solid electrolyte interface (SEI). The corresponding oxidation peaks at 1.5 V and 2.1 V were also found in the CV curves. The subtle curvature at ∼1.5 V may be a very weak peak corresponding to the reverse reaction producing the broad peak in the cathodic sweep (e.g. oxidation of the SEI). CV curves of $Co_9S_8$ nanoparticles (see the Supporting Information, Figure S5) are similar to that of C@$Co_9S_8$ dandelion. But slight diminish of the oxidation peak at ∼2.1 V can be observed that may be due to the slow dissolution of polysulfide and thus some irreversible capacity loss.

The representative discharge−charge voltage profiles (Figure 5b) of C@$Co_9S_8$ dandelion were measured at 1 A $g^{-1}$ in the voltage range of 0.01−3 V. The observed voltage plateaus are consistent with the CV results. The 1st-cycle discharge and charge capacities are 848 and 619 mA h $g^{-1}$, respectively, which results in an irreversible capacity loss of 27%. The relatively high irreversible capacity loss in the 1st cycle is mainly attributed to the irreversible processes including the electrolyte decomposition and inevitable formation of SEI (see the Supporting Information, Figure S6), which are common for nanosized anode materials.[48,49] During the 2nd cycle, the discharge capacity decreases to 636 mA h $g^{-1}$ with a corresponding charge capacity of 602 mA h $g^{-1}$, leading to a much lower irreversible capacity loss of 5%.

Figure 5c displays the comparative cycling performance of C@$Co_9S_8$ dandelions and $Co_9S_8$ nanoparticles at a current density of 1 A $g^{-1}$ (1.8 *C*) between 0.01−3 V. It is clear that C@$Co_9S_8$ dandelions manifest a significantly improved cycling performance as compared to $Co_9S_8$ nanoparticles. For example, the C@$Co_9S_8$ dandelion depicts a much higher specific capacity of 520 mA h $g^{-1}$ during the 50th cycle as compared to only 338 mA h $g^{-1}$ for $Co_9S_8$ nanoparticles. The better cyclability of C@$Co_9S_8$ dandelion is possibly related to the existence of the carbon layer, which may help to reduce the dissolution of polysulfides into the electrolyte. The carbon layer may also effectively buffer the large volume change of $Co_9S_8$ electrode materials during the discharge/charge cycling process.

Good high-*C*-rate performances are desirable for developing LIBs with high power densities. The rate capabilities of both C@$Co_9S_8$ dandelion and $Co_9S_8$ nanoparticles were evaluated at various current densities (Figure 5d). The C@$Co_9S_8$ dandelion depicts the 10th-cycle specific capacities of 563, 506, and 373 mA h $g^{-1}$ at current densities of 2 A $g^{-1}$ (3.6 *C*), 4 A $g^{-1}$ (7.3 *C*) and 6 A $g^{-1}$ (10.9 *C*), respectively. Importantly, after changing the current density from 6 A $g^{-1}$ (10.9 *C*) to 0.2 A $g^{-1}$ (0.4 *C*), the specific capacities of C@$Co_9S_8$ dandelion electrode can recover to >600 mA h $g^{-1}$, implying its good reversibility. The $Co_9S_8$ nanoparticles exhibit much worse rate performance, delivering the 10th-cycle specific capacities of 418, 305, and 111 mA h $g^{-1}$ at current densities of 2 A $g^{-1}$ (3.6 *C*), 4 A $g^{-1}$ (7.3 *C*) and 6 A $g^{-1}$ (10.9 *C*), respectively. The excellent rate performance of C@$Co_9S_8$ dandelion may benefit from its unique 3D open structure, which can effectively buffer the volume strains generated during the Li intercalation/de-intercalation process. And the large specific surface area allows effective contact between the active material and electrolyte while the ultrathin thickness shortens the diffusion paths of charge carriers in the nanostructures.

The better Li storage properties of C@$Co_9S_8$ dandelion as compared to that of $Co_9S_8$ nanoparticles is supported by the electrochemical impedance spectra (EIS) measurements on samples after 3 discharge/charge cycles. The C@$Co_9S_8$ dandelion electrode shows a much smaller radius of semi-circle in the Nyquist plots (Figure 6) as compared to that of the

$Co_9S_8$ nanoparticle electrode. This suggests a lower contact and charge-transfer impedances for the C@$Co_9S_8$ dandelion electrode.[50,51]

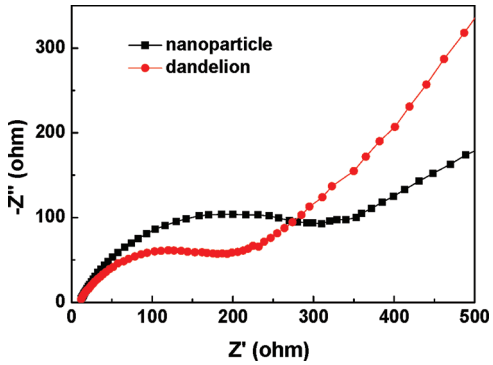


**Figure 6.** Nyquist plots of C@$Co_9S_8$ dandelion and $Co_9S_8$ nanoparticle electrodes after 3 discharge/charge cycles.

## CONCLUSIONS

In conclusion, we demonstrate a novel solvothermal process for the synthesis of carbon coated $Co_9S_8$ nanodandelions using 1-Dodecanethiol as the sulfur source and the soft template. By replacing 1-Dodecanethiol with sulfur powder, 20-nm $Co_9S_8$ nanoparticles without carbon coating are synthesized instead. When tested as LIB anode, the C@$Co_9S_8$ dandelion delivers a specific capacity of 520 mA h $g^{-1}$ at a current density of 1 A $g^{-1}$ (1.8 C) during the 50th cycle, which is much higher than that of $Co_9S_8$ nanoparticles (e.g. 338 mA h $g^{-1}$). Furthermore, the C@$Co_9S_8$ dandelion also exhibits excellent high-C-rate performance, e.g., depicts a 10th-cycle capacity of 373 mA h $g^{-1}$ at a current density of 6 A $g^{-1}$ (10.9 C), which makes it attractive as the anode material to build high-energy-density and high-power-density LIBs.

## ASSOCIATED CONTENT

### Supporting Information

Additional figures are described in the text. This material is available free of charge via the Internet at http://pubs.acs.org/.

## AUTHOR INFORMATION

### Corresponding Author

*E-mail: alexyan@ntu.edu.sg. Tel: +65 6790 4583. Fax: +65 6790 9081.

### Notes

The authors declare no competing financial interest.

## ACKNOWLEDGMENTS

The authors gratefully acknowledge AcRF Tier 1 RG 31/08 of MOE (Singapore), NRF2009EWT-CERP001-026 (Singapore), Singapore Ministry of Education (MOE2010-T2-1-017), A*STAR SERC Grant 1021700144, and Singapore MPA 23/04.15.03 RDP 009/10/102 and MPA 23/04.15.03 RDP 020/10/113 Grant.

## REFERENCES

(1) Etacheri, V.; Marom, R.; Elazari, R.; Salitra, G.; Aurbach, D. *Energy Environ. Sci.* **2011**, *4*, 3243.
(2) Bruce, P. G.; Scrosati, B.; Tarascon, J. M. *Angew. Chem. Int. Ed.* **2008**, *47*, 2930.
(3) Winter, M.; Brodd, R. J. *Chem. Rev.* **2004**, *104*, 4245.
(4) Tarascon, J. M.; Armand, M. *Nature* **2001**, *414*, 359.
(5) Goodenough, J. B.; Kim, Y. *Chem. Mater.* **2009**, *22*, 587.
(6) Long, J. W.; Dunn, B.; Rolison, D. R.; White, H. S. *Chem. Rev.* **2004**, *104*, 4463.
(7) Arico, A. S.; Bruce, P.; Scrosati, B.; Tarascon, J.-M.; van Schalkwijk, W. *Nat. Mater.* **2005**, *4*, 366.
(8) Ji, L.; Lin, Z.; Alcoutlabi, M.; Zhang, X. *Energy Environ. Sci.* **2011**, *4*, 2682.
(9) Liu, C.; Li, F.; Ma, L. P.; Cheng, H. M. *Adv. Mater.* **2010**, *22*, E28.
(10) Hong, L.; Zhaoxiang, W.; Liquan, C.; Xuejie, H. *Adv. Mater.* **2009**, *21*, 4593.
(11) Ye, F.; Wang, C.; Du, G.; Chen, X.; Zhong, Y.; Jiang, J. Z. *J. Mater. Chem.* **2011**.
(12) Cabana, J.; Monconduit, L.; Larcher, D.; Palacín, M. R. *Adv. Mater.* **2010**, *22*, E170.
(13) Kim, Y.; Goodenough, J. B. *J. Phys. Chem. C* **2008**, *112*, 15060.
(14) Du, G.; Guo, Z.; Wang, S.; Zeng, R.; Chen, Z.; Liu, H. *Chem. Commun.* **2010**, *46*, 1106.
(15) Wang, Q.; Li, J. *J. Phys. Chem. C* **2007**, *111*, 1675.
(16) Chang, K.; Chen, W.; Ma, L.; Li, H.; Li, H.; Huang, F.; Xu, Z.; Zhang, Q.; Lee, J. Y. *J. Mater. Chem.* **2011**, *21*, 6251.
(17) Bonneau, P. R.; Jarvis, R. F.; Kaner, R. B. *Nature* **1991**, *349*, 510.
(18) Jang, J. t.; Jeong, S.; Seo, J. w.; Kim, M. C.; Sim, E.; Oh, Y.; Nam, S.; Park, B.; Cheon, J. *J. Am. Chem. Soc.* **2011**, *133*, 7636.
(19) Dong, W.; Wang, X.; Li, B.; Wang, L.; Chen, B.; Li, C.; Li, X.; Zhang, T.; Shi, Z. *Dalton Trans.* **2011**, *40*, 243.
(20) Wang, Q.; Jiao, L.; Han, Y.; Du, H.; Peng, W.; Huan, Q.; Song, D.; Si, Y.; Wang, Y.; Yuan, H. *J. Phys. Chem. C* **2011**, *115*, 8300.
(21) Paolella, A.; George, C.; Povia, M.; Zhang, Y.; Krahne, R.; Gich, M.; Genovese, A.; Falqui, A.; Longobardi, M.; Guardia, P.; Pellegrino, T.; Manna, L. *Chem. Mater.* **2011**, *23*, 3762.
(22) Wu, B.; Song, H.; Zhou, J.; Chen, X. *Chem. Commun.* **2011**, *47*, 8653.
(23) Wang, Z.; Luan, D.; Boey, F. Y. C.; Lou, X. W. *J. Am. Chem. Soc.* **2011**, *133*, 4738.
(24) Ding, S.; Wen Lou, X. *Nanoscale* **2011**, *3*, 3586.
(25) Wang, J. Z.; Zhong, C.; Wexler, D.; Idris, N. H.; Wang, Z. X.; Chen, L. Q.; Liu, H. K. *Chem.—Eur. J.* **2011**, *17*, 661.
(26) Cong, H. P.; Ren, X. C.; Yao, H.-B.; Wang, P.; Cölfen, H.; Yu, S. H. *Adv. Mater.* **2012**, *24*, 1309.
(27) Wu, C. Z.; Xie, Y.; Lei, L. Y.; Hu, S. Q.; OuYang, C. Z. *Adv. Mater.* **2006**, *18*, 1727.
(28) Zhou, W.; Zhu, J.; Cheng, C.; Liu, J.; Yang, H.; Cong, C.; Guan, C.; Jia, X.; Fan, H. J.; Yan, Q.; Li, C. M.; Yu, T. *Energy Environ. Sci.* **2011**.
(29) Wang, H.; Yang, Y.; Liang, Y.; Robinson, J. T.; Li, Y.; Jackson, A.; Cui, Y.; Dai, H. *Nano Lett.* **2011**, *11*, 2644.
(30) Li, X.; Cao, Y.; Qi, W.; Saraf, L. V.; Xiao, J.; Nie, Z.; Mietek, J.; Zhang, J. G.; Schwenzer, B.; Liu, J. *J. Mater. Chem.* **2011**, *21*, 16603.
(31) Guo, J. C.; Xu, Y. H.; Wang, C. S. *Nano Lett.* **2011**, *11*, 4288.
(32) Zheng, G. Y.; Yang, Y.; Cha, J. J.; Hong, S. S.; Cui, Y. *Nano Lett.* **2011**, *11*, 4462.
(33) Liang, C.; Dudney, N. J.; Howe, J. Y. *Chem. Mater.* **2009**, *21*, 4724.
(34) Ji, X.; Lee, K. T.; Nazar, L. F. *Nat. Mater.* **2009**, *8*, 500.
(35) Ji, L.; Rao, M.; Aloni, S.; Wang, L.; Cairns, E. J.; Zhang, Y. *Energy Environ. Sci.* **2011**, *4*, 5053.
(36) Zhou, Y. X.; Yao, H.-B.; Wang, Y.; Liu, H. L.; Gao, M.-R.; Shen, P. K.; Yu, S.-H. *Chem.—Eur. J.* **2010**, *16*, 12000.
(37) Wang, Q.; Jiao, L.; Du, H.; Peng, W.; Han, Y.; Song, D.; Si, Y.; Wang, Y.; Yuan, H. *J. Mater. Chem.* **2011**, *21*, 327.
(38) Yin, Y.; Erdonmez, C. K.; Cabot, A.; Hughes, S.; Alivisatos, A. P. *Adv. Funct. Mater.* **2006**, *16*, 1389.
(39) Liu, B.; Wei, S.; Xing, Y.; Liu, D.; Shi, Z.; Liu, X.; Sun, X.; Hou, S.; Su, Z. *Chem.—Eur. J.* **2010**, *16*, 6625.
(40) Yao, W. T.; Yu, S. H. *Adv. Funct. Mater.* **2008**, *18*, 3357.
(41) Cao, X.; He, Q.; Shi, W.; Li, B.; Zeng, Z.; Shi, Y.; Yan, Q.; Zhang, H. *Small* **2011**, *7*, 1199.

(42) Wang, Q.; Jiao, L.; Du, H.; Yang, J.; Huan, Q.; Peng, W.; Si, Y.; Wang, Y.; Yuan, H. *CrystEngComm* **2011**, *13*, 6960.
(43) Schliehe, C.; Juarez, B. H.; Pelletier, M.; Jander, S.; Greshnykh, D.; Nagel, M.; Meyer, A.; Foerster, S.; Kornowski, A.; Klinke, C.; Weller, H. *Science* **2010**, *329*, 550.
(44) Zhu, J.; Sun, K.; Sim, D.; Xu, C.; Hng, H. H.; Yan, Q. *Chem. Commun.* **2011**, *47*, 10383.
(45) Saadat, S.; Tay, Y. Y.; Zhu, J. X.; Teh, P. F.; Maleksaeedi, S.; Shahjamali, M. M.; Shakerzadeh, M.; Srinivasan, M.; Tay, B. Y.; Hng, H. H.; Ma, J.; Yan, Q. Y. *Chem. Mater.* **2011**, *23*, 1032.
(46) Gomez-Camer, J. L.; Martin, F.; Morales, J.; Sanchez, L. *J. Electrochem. Soc.* **2008**, *155*, A189.
(47) Débart, A.; Dupont, L.; Patrice, R.; Tarascon, J. M. *Solid State Sciences* **2006**, *8*, 640.
(48) Liu, X. H.; Huang, J. Y. *Energy Environ. Sci.* **2011**, *4*, 3844.
(49) Zhu, J. X.; Zhu, T.; Zhou, X. Z.; Zhang, Y. Y.; Lou, X. W.; Chen, X. D.; Zhang, H.; Hng, H. H.; Yan, Q. Y. *Nanoscale* **2011**, *3*, 1084.
(50) Wang, D.; Choi, D.; Li, J.; Yang, Z.; Nie, Z.; Kou, R.; Hu, D.; Wang, C.; Saraf, L. V.; Zhang, J.; Aksay, I. A.; Liu, J. *ACS Nano* **2009**, *3*, 907.
(51) Zhu, J.; Sharma, Y. K.; Zeng, Z.; Zhang, X.; Srinivasan, M.; Mhaisalkar, S.; Zhang, H.; Hng, H. H.; Yan, Q. *J. Phys. Chem. C* **2011**, *115*, 8400.